

Black holes in the long-range limit of torsion bigravity

Vasilisa Nikiforova 

Institut des Hautes Etudes Scientifiques, 91440 Bures-sur-Yvette, France



(Received 12 October 2020; accepted 30 October 2020; published 1 December 2020)

We continue the study of spherically symmetric black hole solutions in torsion bigravity, a class of Einstein-Cartan-type gravity theories involving, besides a metric, a massive propagating torsion field. In the infinite-range limit, these theories admit asymptotically flat black hole solutions related to the presence of attractive fixed points in the asymptotic radial evolution of the metric and the torsion. We discuss these fixed points and the way they are approached at large radii. Several phenomenological aspects of asymptotically flat torsion-hairy black holes are discussed: (i) location of the light ring and of the shadow; (ii) correction to the redshift of orbiting stars; and (iii) modification of the periastron precession of orbiting stars. By comparing the observable properties of torsion-hairy black holes to existing observational data on supermassive black holes obtained by the Event Horizon Telescope Collaboration and by the GRAVITY Collaboration, we derive constraints on the theory parameters of torsion bigravity. The strongest constraint is found to come from the recent measurement of the periastron precession of the star S2 orbiting the Galactic-center massive black hole [R. Abuter et al., *Astron. Astrophys.* **636**, L5 (2020) and to be a thousand times more stringent than Solar-System gravitational tests.

DOI: [10.1103/PhysRevD.102.124007](https://doi.org/10.1103/PhysRevD.102.124007)

I. INTRODUCTION

Black holes (BHs) are one of the most remarkable predictions of Einstein's theory of general relativity (GR). They epitomize GR predictions about strong-field gravity. It is only recently that observational data allowed one to explore in some detail the strong-field structure of BHs. In particular, (i) gravitational-wave data have probed the physics of coalescing, and ringing, BH horizons [1]; (ii) very-long-baseline interferometry has imaged the immediate neighborhood of the supermassive BH at the center of the Messier 87 galaxy [2]; and (iii) the study of stars in highly elliptical orbits around the supermassive BH at the center of our Galaxy has quantitatively checked the strong-field structure of BHs [3,4].

GR has, so far, been found to be compatible with all observational data related to BHs. However, in order to gauge the probing power of various observational windows on BH physics, it is important to be able to compare GR predictions to the predictions of alternative theories of gravity [5]. Actually, there are not many theories of gravity predicting the existence of BHs having regular horizons and a gravitational-field structure different from GR BHs. (Let us, however, recall, following Ref. [6], that even in cases where BH solutions in an alternative theory coincide with GR BHs, their perturbations will generally be different from the GR ones and, thereby, lead to different observable predictions.) For examples of BHs in alternative theories of gravity, see Refs. [7–12].

In a recent work [13], we have explored the existence and structure of (spherically symmetric) BHs in *torsion*

bigravity. This theory generalizes (*à la* Cartan) GR by adding to the Einstein metric field $g_{\mu\nu}$ an independent affine connection $A^\lambda{}_{\mu\nu}$, having a nonzero torsion tensor $T^\lambda{}_{[\mu\nu]}$. General classes of ghost-free and tachyon-free theories involving a propagating torsion were introduced long ago [14–19]. Torsion bigravity is a specific, minimal class of dynamical-torsion theory containing only two excitations: a massless, GR-type spin-2 excitation and a massive spin-2 one. In other words, torsion bigravity has the same excitation content as (ghost-free) bimetric gravity [20]. Previous work (notably, Refs. [21–23]) has indicated that torsion bigravity seems to define a viable alternative theory of gravity, endowed with purely geometric structures and having interesting physical properties.

In the present work, we complete the study of Ref. [13] by exploring in detail the structure of the *asymptotically flat torsion-hairy* black holes, which were found to exist in the infinite-range limit of torsion bigravity. General torsion-bigravity theories contain four parameters, denoted c_R , c_F , c_{F^2} , and c_{34} in Ref. [22]. The latter parameter does not influence the spherically symmetric sector. We are then left with three parameters that are conveniently parametrized in terms of (i) a dimensionful parameter $\lambda \equiv c_F + c_R = \frac{1}{16\pi G_0}$, measuring the gravitational coupling of the massless spin-2 excitation; (ii) the dimensionless parameter $\eta \equiv c_F/c_R$ measuring the ratio between the coupling of the massive spin-2 field and the coupling of the massless spin-2 one; and (iii) the inverse range (or Compton wavelength) $\kappa \equiv \sqrt{\eta\lambda/c_{F^2}}$ of the massive spin-2 excitation. With this notation, the Lagrangian density of torsion bigravity reads

$$L = \frac{\lambda}{1+\eta}R + \frac{\eta\lambda}{1+\eta}F + \frac{\eta\lambda}{\kappa^2} \left(F_{(\mu\nu)}F^{(\mu\nu)} - \frac{1}{3}F^2 \right). \quad (1.1)$$

Here, R denotes the usual scalar curvature of $g_{\mu\nu}$, while $F \equiv g^{\mu\nu}F_{\mu\nu}$, where $F_{\mu\nu}$ denotes the Ricci tensor of the metric-preserving, but torsionful, affine connection $A^\lambda_{\mu\nu}$. For the convenience of the reader, the full definitions of these objects are summarized in the Appendix A.

The long-range limit $\kappa \rightarrow 0$ looks *a priori* singular for the Lagrangian (1.1). (As discussed in Ref. [22], this formal limit might physically correspond to the case where κ is of the order of the Hubble scale H_0 .) However, it was proven in Ref. [23] that the spherically symmetric field equations, and solutions, of torsion bigravity admit a smooth limit as $\kappa \rightarrow 0$. This smoothness emerges when using suitable variables and, notably, the variable denoted $\bar{\pi}$. See Appendix B for the explicit form of the (spherically symmetric) field equations of torsion bigravity, on which one can explicitly see the smoothness of the long-range limit $\kappa \rightarrow 0$.

Reference [13] has found that, in the infinite-range limit, $\kappa \rightarrow 0$, there existed *asymptotically flat* BHs, having regular horizons and endowed with an asymptotically decaying, horizon-regular torsion field $T^\lambda_{[\mu\nu]}$. These solutions are parametrized, besides the dimensionless theory parameter¹ η , by the (areal) radius r_h of the BH and by the dimensionless parameter $\bar{\pi}_0$, measuring the horizon value of the following (κ^2 -rescaled) combination of frame components of the curvature tensor $F^\lambda_{\mu\nu\rho}$ of the torsionful connection $A^\lambda_{\mu\nu}$ (see Appendix A for the detailed definition of $F^\lambda_{\mu\nu\rho}$):

$$\bar{\pi} = \kappa^{-2}(F_{\hat{0}\hat{1}\hat{0}\hat{1}} + F_{\hat{1}\hat{2}\hat{1}\hat{2}} - F_{\hat{0}\hat{2}\hat{0}\hat{2}} - F_{\hat{2}\hat{3}\hat{2}\hat{3}}). \quad (1.2)$$

Those asymptotically flat, torsion-hairy BHs were obtained by proving the existence of fixed points, when $r \rightarrow \infty$, of the system of three first-order ordinary differential equations (ODEs) describing the radial evolution (from the horizon up to spatial infinity) of the geometric structure $g_{\mu\nu}$, $T^\lambda_{[\mu\nu]}$. In the following, we shall successively (i) discuss (in Sec. II) all the fixed points of the latter system of ODEs and their main properties; (ii) focus (in Sec. III) on the properties of the particular fixed point that yields asymptotically flat BHs; and, finally, (iii) study (in Sec. IV) the phenomenology of the latter asymptotically flat torsion-hairy BHs and compare some of the physical effects they predict to the observational results on the star S2, which orbits the supermassive BH at the center of our Galaxy [3,4].

¹The dimensionful gravitational-coupling parameter λ does not enter these vacuum solutions.

II. ASYMPTOTIC FIXED POINTS OF THE RADIAL EVOLUTION SYSTEM

Spherically symmetric solutions of torsion bigravity are described by four variables: $\Phi(r)$, $L(r)$, $V(r)$, and $W(r)$. The first two variables, $\Phi(r)$ and $L(r)$, describe the metric:

$$ds^2 = -e^{2\Phi} dt^2 + L^2 dr^2 + r^2(d\theta^2 + \sin^2\theta d\phi^2). \quad (2.1)$$

The last two, $V(r)$ and $W(r)$, describe the independent components of the torsionful connection \mathbf{A} in the polar-type vierbein $e^{\hat{\mu}}$ defined by the metric (2.1). Namely (see Appendix A for details),

$$V = A^{\hat{1}}_{\hat{0}\hat{0}} \quad (2.2)$$

and

$$W = A^{\hat{1}}_{\hat{2}\hat{2}} = A^{\hat{1}}_{\hat{3}\hat{3}}. \quad (2.3)$$

It is then convenient to further introduce the auxiliary variables $F(r) \equiv \Phi'(r)$ (where the prime denotes a radial derivative) and $\bar{\pi}(r)$, defined by Eq. (1.2), which means that $\bar{\pi}$ is linear in the radial derivatives of $V(r)$ and $W(r)$ [see Eq. (4.3) of Ref. [13]]. It was shown in Refs. [13,22,23] that the five variables $F(r)$, $L(r)$, $V(r)$, $W(r)$, and $\bar{\pi}(r)$ then satisfy a system of ODEs which can be reduced to (i) two algebraic equations that can be solved to express F and V in terms of $L(r)$, $W(r)$, and $\bar{\pi}(r)$ and (ii) a system of three first-order ODEs describing the radial evolution of the three variables [$L(r)$, $W(r)$, and $\bar{\pi}(r)$]. When discussing BH solutions, it is convenient to replace the three variables [$L(r)$, $W(r)$, and $\bar{\pi}(r)$] by the equivalent set

$$(X^1, X^2, X^3) \equiv (\tilde{l}, \tilde{w}, \bar{\pi}). \quad (2.4)$$

Here \tilde{l} and \tilde{w} are defined as

$$\tilde{l}(r) \equiv \frac{L(r)}{L_S(r)} \quad \text{and} \quad \tilde{w}(r) \equiv \frac{W(r)}{W_S(r)}, \quad (2.5)$$

respectively, where L_S and W_S are the values of L and W for a Schwarzschild BH. We recall (see [13]) that the geometric structure ($g_{\mu\nu}$, $A^\lambda_{\mu\nu}$) of a Schwarzschild BH is described by the variables

$$\begin{aligned} \Phi_S(r) &= +\frac{1}{2} \ln \left(1 - \frac{r_h}{r} \right), \\ F_S(r) &= +\frac{1}{2} \frac{r_h}{r(r-r_h)}, \\ L_S(r) &= \left(1 - \frac{r_h}{r} \right)^{-1/2}, \\ V_S(r) &= \frac{F_S(r)}{L_S(r)} = \frac{1}{2} \frac{r_h}{r^2} \left(1 - \frac{r_h}{r} \right)^{-1/2}, \\ W_S(r) &= -\frac{1}{rL_S(r)} = -\frac{1}{r} \left(1 - \frac{r_h}{r} \right)^{1/2}, \\ \bar{\pi}_S(r) &= -3 \frac{r_h}{\kappa^2 r^3}. \end{aligned} \quad (2.6)$$

The three variables X^i , $i = 1, 2, 3$ [Eq. (2.4)], satisfy a first-order radial evolution system, say,

$$\frac{dX^i}{dr} = F^i(r, X^j). \quad (2.7)$$

The explicit form of this system can be read off by taking the limit $\kappa \rightarrow 0$ in Eqs. (B2) of Appendix B.

The large- r asymptotics of the latter system yields a Fuchsian-type system, of the form

$$\frac{d}{dr}X^i = \frac{1}{r}V^i(X^j) + O\left(\frac{1}{r^2}\right). \quad (2.8)$$

Neglecting the $O(\frac{1}{r^2})$ subleading correction and introducing $\rho \equiv \ln r$ leads to a vectorial flow equation for the ρ -evolution of the point \mathbf{X} in a three-dimensional space:

$$\frac{d}{d\rho}X^i = V^i(X^j). \quad (2.9)$$

Let us consider the solutions \mathbf{X}_∞ of the three (algebraic) equations

$$V^i(X_\infty^j) = 0. \quad (2.10)$$

These solutions define the *fixed points* of the vectorial flow (2.9): If the system (2.9) crosses a state corresponding to any of its fixed points, it will stay there forever:

$$\frac{d}{d\rho}X_\infty^i = V^i(X_\infty^j) = 0. \quad (2.11)$$

Yet this does not tell anything about the *accessibility* of the fixed points. The first issue to understand, for knowing whether the system can reach a certain fixed point, is to assess whether this fixed point is an attractor or not. Let us recall the relevant mathematics. We consider a small perturbation $\xi^i(\rho)$ around a fixed point:

$$X^i(\rho) = X_\infty^i + \epsilon \xi^i(\rho). \quad (2.12)$$

Substituting the latter expression in Eq. (2.9) and making a series expansion of the right-hand side up to the linear order, one obtains the following equation, describing linear perturbations around any fixed point:

$$\frac{d}{d\rho}\xi_{\text{lin}}^i(\rho) = \left[\frac{\partial V^i}{\partial X^j}\right](\mathbf{X}_\infty)\xi_{\text{lin}}^j(\rho) = J_j^i(\mathbf{X}_\infty)\xi_{\text{lin}}^j(\rho). \quad (2.13)$$

Here

$$J_j^i(\mathbf{X}_\infty) \equiv \left[\frac{\partial V^i}{\partial X^j}\right](\mathbf{X}_\infty) \quad (2.14)$$

denotes the Jacobian matrix of the system (2.9); it is made of the partial derivatives of the functions V^i with respect

to $X^j = \{\tilde{l}, \tilde{w}, \tilde{\pi}\}$ taken at the fixed point $\mathbf{X}_\infty = \{\tilde{l}_\infty, \tilde{w}_\infty, \tilde{\pi}_\infty\}$.

To obtain the law of evolution of the linear perturbations, one introduces the eigenvectors $E_{(n)}^i$, $n = 1, 2, 3$, of the matrix J_j^i , say,

$$J_j^i E_{(n)}^j = \lambda_{(n)} E_{(n)}^i, \quad (2.15)$$

and decomposes ξ_{lin}^i along the vector basis of eigenvectors, say,

$$\xi_{\text{lin}}^i(\rho) = \sum_n \delta_{(n)}(\rho) E_{(n)}^i, \quad (2.16)$$

where it should be noted that the eigenvectors $E_{(n)}^i$ do not depend on ρ . Inserting Eq. (2.16) into Eq. (2.13), one obtains the ρ -evolution law for the coefficients $\delta_{(n)}(\rho)$:

$$\frac{d}{d\rho}\delta_{(n)}(\rho) = \lambda_{(n)}\delta_{(n)}(\rho). \quad (2.17)$$

This gives the following equation describing the evolution of general linear perturbations ξ_{lin}^i around a fixed point:

$$\xi_{\text{lin}}^i(\rho) = \sum_n c_{(n)} e^{\lambda_{(n)}\rho} E_{(n)}^i = \sum_n C_{(n)}^i e^{\lambda_{(n)}\rho}, \quad (2.18)$$

where $c_{(n)}$ and $C_{(n)}^i$ are some constants, depending on the initial values for $\xi_{\text{lin}}^i(\rho)$.

The first conclusion is that the attractive or repulsive character of a fixed point is determined by the eigenvalues of Jacobian matrix: A fixed point is an attractor (and all the trajectories from a small neighborhood of the fixed point will end up at the fixed point) if the real parts of all the eigenvalues $\lambda_{(n)}$ are *negative*.

In addition, we must remember that our exact radial evolution system [Eq. (2.7)] is to be integrated with restricted initial conditions on the horizon, $r = r_h$. Indeed, Ref. [13] has shown that a single shooting parameter (namely, $\tilde{\pi}_0$) can be specified on the horizon. Then the following radial evolution (from $r = r_h$ up to $r = +\infty$) of the three variables $X^i = \{\tilde{l}, \tilde{w}, \tilde{\pi}\}$ will depend on $\tilde{\pi}_0$, on r_h , and on the theory parameter η . (As in Ref. [13], we often use, for convenience, units where $r_h = 1$.) Therefore, besides analytically studying the attractor nature of the fixed points, we shall need numerical simulations to check whether the one-parameter family of horizon initial values can belong to the basin of attraction of any given attractive fixed point.

A. List of asymptotic fixed points of the radial evolution

Let us now go to practice and analyze all the fixed points of the system (2.10). This algebraic system gives ten fixed points. Five of them are characterized by $\tilde{l}_\infty < 0$ and, thus,

are nonphysical, so we will not consider them. We must indeed remember at this stage that the physical meaning of the variable $X^1 = \tilde{l}$, defined in Eq. (2.5), is such that we need to impose $\tilde{l}(r) > 0$. We will discuss below the further conditions characterizing *asymptotically flat* BH solutions.

Among the remaining five points, one is only partially attractive: The fixed point $(\tilde{l}_\infty = 1, \tilde{w}_\infty = 1, \tilde{\pi}_\infty = 0)$ has eigenvalues $\lambda_{(n)} = (-1, -3, 2)$, so that it is repulsive in one eigendirection.

Let us consider more in detail the four remaining fixed points.

- (i) The most interesting is the fixed point

$$\left(\tilde{l}_\infty = 1, \tilde{w}_\infty = -1, \tilde{\pi}_\infty = \frac{6}{1+\eta} \right), \quad (2.19)$$

describing the *asymptotically flat torsion-hairy*² black hole solution which was discussed in the previous paper [13] (see Sec. X there). The corresponding eigenvalues are

$$\lambda_{(n)} = \left\{ -1, -\frac{1}{2} + i\frac{\sqrt{7}}{2}, -\frac{1}{2} - i\frac{\sqrt{7}}{2} \right\}. \quad (2.20)$$

The real parts of the eigenvalues displayed in Eq. (2.20) are all strictly negative. This shows that the fixed point (2.19) is a (local) attractor.

The analytical expressions of \tilde{l}_∞ , \tilde{w}_∞ , and $\tilde{\pi}_\infty$ for the three remaining fixed points are rather complicated, so we will use a numerical description. They all correspond to *non asymptotically flat torsion-hairy black hole solutions*.

- (i) The second fixed point *exists only for* $\eta > 1/3$, because the values of $\eta < 1/3$ give imaginary values for \tilde{l}_∞ , \tilde{w}_∞ , and $\tilde{\pi}_\infty$. For all $\eta > 1/3$, it is an attractive fixed point. The latter fact was checked numerically by computing the eigenvalues. When η varies from $1/3$ to infinity, the value of \tilde{l}_∞ respectively varies in the interval

$$\sqrt{2} < \tilde{l}_\infty < \sqrt{3}. \quad (2.21)$$

The fact that $\tilde{l}_\infty > 1$ means that the corresponding BH is non asymptotically flat. Figure 1 shows the spectrum of values of \tilde{l}_∞ , \tilde{w}_∞ , and $\tilde{\pi}_\infty$ as a function of the theory parameter η .

- (ii) The third fixed point also *makes sense only for* $\eta > 1/3$, and it is an attractive fixed point for all $\eta > 1/3$. When η varies from $1/3$ to infinity, the value of \tilde{l}_∞ decreases from $\tilde{l}_\infty(\eta = 1/3) = \sqrt{2}$ to $\tilde{l}_\infty(\eta \rightarrow +\infty) = 1.3$. Figure 2 shows the spectrum of values of \tilde{l}_∞ , \tilde{w}_∞ , and $\tilde{\pi}_\infty$ as a function of η .

²Note that the condition $\tilde{l}_\infty = 1$ is necessary for the asymptotic flatness of the metric.

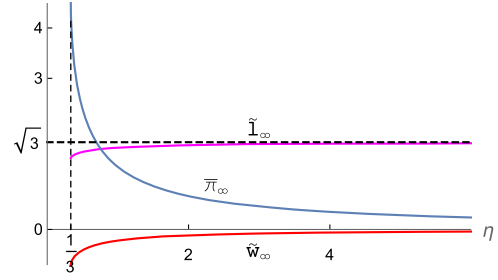


FIG. 1. Fixed point values \tilde{l}_∞ , \tilde{w}_∞ , and $\tilde{\pi}_\infty$ for the second fixed point. The value of \tilde{w}_∞ varies between $\tilde{w}_\infty(\eta = \frac{1}{3}) = -1/\sqrt{2}$ and $\tilde{w}_\infty(\eta \rightarrow \infty) = 0$. The value of $\tilde{\pi}_\infty$ varies between $\tilde{\pi}_\infty(\eta = \frac{1}{3}) = \frac{9}{2}$ and $\tilde{\pi}_\infty(\eta \rightarrow +\infty) = 0$.

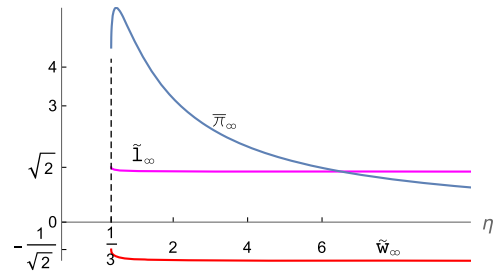


FIG. 2. Fixed point values \tilde{l}_∞ , \tilde{w}_∞ , and $\tilde{\pi}_\infty$ for the third fixed point. The value of \tilde{w}_∞ varies between $\tilde{w}_\infty(\eta = \frac{1}{3}) = -1/\sqrt{2}$ and $\tilde{w}_\infty(\eta \rightarrow +\infty) = -1$. The value of $\tilde{\pi}_\infty$ varies between $\tilde{\pi}_\infty(\eta = \frac{1}{3}) = \frac{9}{2}$ and $\tilde{\pi}_\infty(\eta \rightarrow +\infty) = 0$.

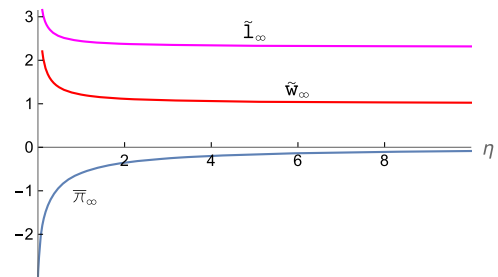


FIG. 3. Fixed point values \tilde{l}_∞ , \tilde{w}_∞ , and $\tilde{\pi}_\infty$ for the fourth fixed point. The value of \tilde{w}_∞ varies between $\tilde{w}_\infty(\eta \rightarrow 0) \rightarrow +\infty$ and $\tilde{w}_\infty(\eta \rightarrow \infty) = 1$. The value of $\tilde{\pi}_\infty$ varies between $\tilde{\pi}_\infty(\eta \rightarrow 0) \rightarrow +\infty$ and $\tilde{\pi}_\infty(\eta \rightarrow +\infty) = 0$.

- (iii) The last, fourth fixed point makes sense for all η 's, and it is attractive. The value of \tilde{l}_∞ varies from $\tilde{l}_\infty(\eta \rightarrow 0) \rightarrow +\infty$ to $\tilde{l}_\infty(\eta \rightarrow +\infty) = 2.3$. See Fig. 3 for more details.

III. ASYMPTOTICALLY FLAT TORSION-HAIRY BHS IN THE LARGE-RANGE LIMIT

Let us now analyze in some detail the asymptotically flat torsion-hairy BHs obtained with the first fixed point, i.e.,

$$\mathbf{X}_\infty = (\tilde{l}_\infty, \tilde{w}_\infty, \tilde{\kappa}_\infty) = \left(1, -1, \frac{6}{\eta+1}\right). \quad (3.1)$$

As already mentioned, the approach toward this fixed point is characterized by the three η -independent eigenvalues

$$\lambda_{(n)} = \left\{-1, -\frac{1}{2} + i\frac{\sqrt{7}}{2}, -\frac{1}{2} - i\frac{\sqrt{7}}{2}\right\}. \quad (3.2)$$

Inserting (2.20) into (2.18) and taking into account that we are considering real solutions of the real perturbation equation (2.13), we get, for a general real asymptotic solution, the form

$$\xi_{\text{lin}}^i(\rho) = C_{(1)}^i e^{-\rho} + C_{(2)}^i e^{-\rho/2} e^{i(\sqrt{7}/2)\rho} + [C_{(2)}^i e^{-\rho/2} e^{-i(\sqrt{7}/2)\rho}]^*, \quad (3.3)$$

where $C_{(1)}^i$ is real and where $*$ means complex conjugation. This gives, in more explicit form,

$$\xi_{\text{lin}}^i(\rho) = 2|C_{(2)}^i| e^{-\rho/2} \cos\left(\frac{\sqrt{7}}{2}\rho + \Phi^i\right) + C_{(1)}^i e^{-\rho}, \quad (3.4)$$

where Φ^i are some phases. In terms of r (remembering that $\rho \equiv \ln r$), this looks as follows:

$$\xi_{\text{lin}}^i(r) = \frac{2|C_{(2)}^i|}{r^{1/2}} \cos\left(\frac{\sqrt{7}}{2} \ln r + \Phi^i\right) + \frac{C_{(1)}^i}{r}. \quad (3.5)$$

At this point, we should note that the perturbations ξ_{lin}^i were obtained in the linearized approximation. In other words, Eq. (3.5) neglected the contributions coming from terms quadratic (and higher) in ξ in the perturbation equation. Instead of solving Eq. (2.13), we should have solved a nonlinear equation of the form

$$\frac{d}{d\rho} \xi_{\text{nonlin}}^i = J^i_j \xi_{\text{nonlin}}^j + J^i_{jk} \xi_{\text{nonlin}}^j \xi_{\text{nonlin}}^k + \dots \quad (3.6)$$

Let us sketch the structure of the corrections to the linearized solution (3.5) when considering only the quadratically nonlinear terms and treating them perturbatively, i.e., solving the equation

$$\frac{d}{d\rho} \xi_{\text{nonlin}}^i = J^i_j \xi_{\text{nonlin}}^j + J^i_{jk} \xi_{\text{lin}}^j \xi_{\text{lin}}^k, \quad (3.7)$$

where ξ_{lin}^i is given by (3.4). The structure of the last, quadratic term in Eq. (3.7) is

$$\begin{aligned} J^i_{jk} \xi_{\text{lin}}^j \xi_{\text{lin}}^k &= J^i_{jk} \left(\sum_n C_{(n)}^j e^{\lambda_{(n)}\rho} \right) \left(\sum_m C_{(m)}^k e^{\lambda_{(m)}\rho} \right) \\ &= \tilde{C}_1^i e^{-\rho} + \tilde{C}_{2+}^i e^{(-1+i\sqrt{7})\rho} + \tilde{C}_{2-}^i e^{(-1-i\sqrt{7})\rho} \\ &\quad + \tilde{C}_{3+}^i e^{[-(3/2)+i(\sqrt{7}/2)]\rho} \\ &\quad + \tilde{C}_{3-}^i e^{[-(3/2)-i(\sqrt{7}/2)]\rho} + \tilde{C}_4^i e^{-2\rho}. \end{aligned} \quad (3.8)$$

Among the contributions contained in this quadratically nonlinear ‘‘source term,’’ the term

$$\tilde{C}_1^i e^{-\rho}$$

coincides with a fundamental solution of the homogeneous equation (2.13) with $\lambda_{(n)} = \lambda_{(1)} = -1$. As a consequence, such a resonant source term will generate a solution of (3.7) of the type $e^{-\rho}$. The other, nonresonant, terms in (3.8) will generate exponential solutions of the same form as they are: The terms $e^{(-1\pm i\sqrt{7})\rho}$ after taking the real part will generate in the solution a term of the type $e^{-\rho} \cos(\sqrt{7}\rho + \text{phase})$, while the terms $e^{[-(3/2)\pm i(\sqrt{7}/2)]\rho}$ will generate a term of the type $e^{-3\rho/2} \cos(\frac{\sqrt{7}}{2}\rho + \text{phase})$. Finally, the quadratically nonlinear solution for ξ^i will have the following structure:

$$\begin{aligned} \xi^i(\rho) &= C_{[(1/2)\cos]}^i e^{-\rho/2} \cos\left(\frac{\sqrt{7}}{2}\rho + \Phi_{(1/2)}^i\right) \\ &\quad + C_{(1)}^i e^{-\rho} + C_{(\ln)}^i e^{-\rho} \\ &\quad + C_{(\cos)}^i e^{-\rho} \cos(\sqrt{7}\rho + \Phi_{(1)}^i) + O(e^{-3\rho/2}), \end{aligned} \quad (3.9)$$

or, in terms of r ,

$$\begin{aligned} \xi^i(r) &= \frac{C_{[(1/2)\cos]}^i}{r^{1/2}} \cos\left(\frac{\sqrt{7}}{2} \ln r + \Phi_{(1/2)}^i\right) + \frac{C_{(1)}^i}{r} \\ &\quad + \frac{C_{(\ln)}^i \ln r}{r} + \frac{C_{(\cos)}^i}{r} \cos(\sqrt{7} \ln r + \Phi_{(1)}^i) \\ &\quad + O(r^{-3/2}). \end{aligned} \quad (3.10)$$

This gives the following expression for the large- r behavior of $\mathbf{X} = (\tilde{l}, \tilde{w}, \tilde{\kappa})$:

$$\begin{aligned} X^i(r) &= X_\infty^i + \frac{C_{[(1/2)\cos]}^i}{r^{1/2}} \cos\left(\frac{\sqrt{7}}{2} \ln r + \Phi_{(1/2)}^i\right) \\ &\quad + \frac{C_{(1)}^i}{r} + \frac{C_{(\ln)}^i \ln r}{r} + \frac{C_{(\cos)}^i}{r} \cos(\sqrt{7} \ln r + \Phi_{(1)}^i) \\ &\quad + O(r^{-3/2}). \end{aligned} \quad (3.11)$$

The last expression gives, for example, the following behavior of $\sqrt{g_{rr}} = L = \tilde{l}/\sqrt{1 - r_h/r}$ near infinity:

$$\begin{aligned} \sqrt{g_{rr}} &= 1 + \frac{C_{[(1/2)\cos]}^l}{r^{1/2}} \cos\left(\frac{\sqrt{7}}{2} \ln r + \Phi_{(1/2)}^l\right) + \frac{C_{(1)}^l}{r} \\ &+ \frac{C_{(\ln)}^l \ln r}{r} + \frac{C_{(\cos)}^l}{r} \cos(\sqrt{7} \ln r + \Phi_{(1)}^l) \\ &+ O(r^{-3/2}). \end{aligned} \quad (3.12)$$

When comparing this asymptotic behavior to the usual Schwarzschild one, namely,

$$\sqrt{g_{rr}^S} = \frac{1}{\sqrt{1 - r_h/r}} = 1 + \frac{r_h}{2r} + O(r^{-2}), \quad (3.13)$$

the most striking difference is the fact that the leading term in the large- r expansion of $\sqrt{g_{rr}}$ is not decaying as $O(r^{-1})$ but decays in the slower $O(r^{-1/2})$ manner and, moreover, presents oscillations on the logarithmic scale $\ln r$, with a universal frequency $\frac{\sqrt{7}}{2}$. By computing the corresponding solution for the potential $\Phi(r) = \frac{1}{2} \ln |g_{00}|$ describing the time-time component of the metric in torsion bigravity, one similarly finds that the leading term in the large- r expansion of $\Phi(r)$ also contains an oscillating, slowly decaying piece $\propto r^{-1/2} \cos(\frac{\sqrt{7}}{2} \ln r + \text{phase})$. The physical consequences of such slowly decaying (and oscillating) contributions are discussed in the following subsections.

A. Expansion of the BH solution in powers of η

Let us show that, in the formal limit $\eta \rightarrow 0$, the metric structure [described by the functions $L(r)$ and $F(r) = \Phi'(r)$] of asymptotically flat BHs tend to the Schwarzschild one $L = L_S$ and $F = F_S$ [defined in Eqs. (2.6)].

To this end, we first remark that Eq. (B3) becomes very simple in the limit $\eta = 0$ (with $\kappa = 0$). One finds that it takes the following form:

$$\tilde{l}' = \frac{\tilde{l}(1 - \tilde{l}^2)}{2(r-1)}. \quad (3.14)$$

We should solve this equation taking into account the boundary conditions at the horizon which were discussed in Ref. [13]. Looking at Eqs. (7.8)–(7.10) of Ref. [13], one can see that, in the limit $\eta \rightarrow 0$, the horizon value $\tilde{l}(r = r_h) \rightarrow 1$, independently of the value chosen for the free shooting parameter $\tilde{\pi}_0$. Since the right-hand side of Eq. (3.14) equals zero when $\tilde{l} = 1$, the unique solution which satisfies the boundary conditions is found to be

$$\tilde{l}(r) \equiv 1 \quad (\text{when } \eta \rightarrow 0). \quad (3.15)$$

Inserting this result (together with $\kappa = 0$ and $\eta = 0$) in Eqs. (B4) and (B2), one then finds that the radial behavior of \tilde{w} and $\tilde{\pi}$ is described by the following system of two first-order equations:

$$\begin{aligned} r\tilde{w}' &= -\frac{\tilde{\pi}^2 + 3\tilde{\pi}(2 - r + r\tilde{w}) - 9(2 - 2r + (2r - 3)\tilde{w})}{3(r-1)(3 + \tilde{\pi})}, \\ r\tilde{\pi}' &= 3 - 2\tilde{\pi} - 3\tilde{w} - \tilde{\pi}\tilde{w}. \end{aligned} \quad (3.16)$$

The large- r limit of this system is a two-dimensional Fuchsian system which admits, as a fixed point, the values $(\tilde{w}_\infty, \tilde{\pi}_\infty) = (-1, 6)$. These values are the two-dimensional projection of the $\eta = 0$ limit of the fixed point (3.1). The corresponding two-dimensional Jacobian matrix is found to have the eigenvalues

$$\lambda_{(1,2)} = -\frac{1}{2} \pm i \frac{\sqrt{7}}{2}. \quad (3.17)$$

Similarly to the previous section, we can conclude from this the following law of asymptotic approach to the fixed point:

$$\tilde{w}_{\eta 0}(r) = -1 + \frac{A_w}{r^{1/2}} \cos\left(\frac{\sqrt{7}}{2} \ln r + \Phi_w\right), \quad (3.18)$$

$$\tilde{\pi}_{\eta 0}(r) = 6 + \frac{A_\pi}{r^{1/2}} \cos\left(\frac{\sqrt{7}}{2} \ln r + \Phi_\pi\right), \quad (3.19)$$

plus some terms of higher orders in $1/r$. Here, the constants A_w and A_π depend on the integration constants of the system (3.16).

Finally, putting $\eta = 0$ and $\kappa = 0$ and inserting Eqs. (3.15), (3.18), and (3.19) into the algebraic equation (B1) giving F in terms of \tilde{l} , \tilde{w} , and $\tilde{\pi}$, one finds that

$$F|_{\eta=0, \kappa=0} = F_S, \quad (3.20)$$

where $F_S = \frac{1}{2(r-1)r}$ is the Schwarzschild value.

Having determined the structure of the solution in the limit $\eta \rightarrow 0$, we can now discuss the structure of the solutions when η is nonzero, but small. Let us indeed recall that Ref. [22] has studied the phenomenological constraints on the torsion-bigravity theory parameter η in the limit $\kappa \rightarrow 0$ and has concluded that Solar-System gravity tests constrain η to be small; more precisely [see Eq. (10.18) in Ref. [22]],

$$\eta \lesssim 10^{-5} \quad (\text{from Solar-System gravitational tests}). \quad (3.21)$$

It is then appropriate to work only linearly in η . We then conclude from the result (3.15) that

$$\tilde{l}(r) \equiv 1 + \eta \tilde{l}_1(r) + O(\eta^2). \quad (3.22)$$

One then gets a differential equation for $\tilde{l}_1(r)$ by inserting the expansion (3.22) in Eq. (B3), working at linear order in η . Together with Eq. (B3), this gives

$$\tilde{l}'_1 = -\frac{\tilde{l}_1}{r-1} + f_l(\tilde{w}_{\eta 0}, \tilde{\pi}_{\eta 0}) + O(\eta), \quad (3.23)$$

where f_l is a polynomial function of its arguments (and a rational function of r). Replacing $\tilde{w}_{\eta 0}$ and $\tilde{\pi}_{\eta 0}$ by solutions of the system (3.16) then yields an inhomogeneous first-order ODE determining the radial evolution of \tilde{l}_1 . In particular, we can obtain the asymptotic radial behavior of \tilde{l}_1 by substituting in Eq. (3.23) the asymptotic expansions Eqs. (3.18) and (3.19). We thereby obtain an inhomogeneous differential equation of the form

$$\tilde{l}'_1 = -\frac{\tilde{l}_1}{r-1} - \frac{3}{r(r-1)} + f_{l\cos}(r) + O(\eta), \quad (3.24)$$

where $f_{l\cos}(r)$ is a sum of terms involving oscillatory factors and powers of r . Solving the resulting equation yields the following expression for \tilde{l}_1 :

$$\begin{aligned} \tilde{l}_1(r) &= \frac{A_{[l,(1/2)\cos]}}{r^{1/2}} \cos\left(\frac{\sqrt{7}}{2} \ln r + \Phi^{l2}\right) \\ &+ \frac{1}{r} [A_{(l,1)} + A_{(l,\ln)} \ln r \\ &+ A_{(l,\cos)} \cos(\sqrt{7} \ln r + \Phi^{l1})] + O(\eta). \end{aligned} \quad (3.25)$$

This form of $\tilde{l}_1(r)$ is in agreement with the arguments of the beginning of this section [see Eq. (3.10)] concerning the form of perturbations around the fixed point (2.20). Indeed, one can see the oscillatory behavior which becomes dominant for large r .

However, the new information we got from the reasoning of the present section is that the unusual slowly decaying, oscillatory contributions enter the metric function \tilde{l} (and, therefore, $L = L_S \tilde{l}$) *only at the $O(\eta)$ level*, because $\tilde{l} = 1 + \eta \tilde{l}_1 + O(\eta^2)$. It is phenomenologically important to discuss also how these unusual slowly decaying oscillatory contributions enter the other metric function, namely, $g_{00} = -e^{2\Phi}$, or the related function $F = \Phi'$. As we showed above that $\lim_{\eta \rightarrow 0} F = F_S$, we immediately see that the unusual slowly decaying oscillatory contributions will also enter F , and thereby Φ , only at the $O(\eta)$ level.

More precisely, considering the series expansion in η of Eq. (B1) for F one obtains an expression of the type

$$F = F_S + \eta f_F(\tilde{l}_1, \tilde{w}_{\eta 0}, \tilde{\pi}_{\eta 0}) + O(\eta^2), \quad (3.26)$$

where f_F is a polynomial function of its arguments. Substituting in this expression the asymptotic behavior of the various arguments, namely, Eqs. (3.18) and (3.19) for $\tilde{w}_{\eta 0}$ and $\tilde{\pi}_{\eta 0}$ and Eq. (3.25) for \tilde{l}_1 , one finds that the asymptotic radial behavior of $F(r)$ is of the form

$$\begin{aligned} F(r) &= F_S + \eta \left\{ \frac{A_{[F,(1/2)\cos]}}{r^{3/2}} \cos\left(\frac{\sqrt{7}}{2} \ln r + \hat{\Phi}^{F2}\right) \right. \\ &+ \frac{1}{r^2} [A_{(F,1)} + A_{(F,\ln)} \ln r \\ &+ \hat{A}_{(F,\cos)} \cos(\sqrt{7} \ln r + \hat{\Phi}^{F1})] \left. \right\} + O(\eta^2). \end{aligned} \quad (3.27)$$

Having in hand such an explicit form of the asymptotic behavior of $F(r)$, one can now discuss the physical consequences of having such slowly decaying (and oscillating) contributions. More precisely, we can estimate the order of magnitude of the ‘‘crossing distance,’’ say, r_\times , where the oscillatory contributions in F [i.e., the terms $\propto \eta r^{-3/2} \cos(\frac{\sqrt{7}}{2} \ln r + \hat{\Phi}^{F2})$ in Eq. (3.27)] start to dominate over the usual, Schwarzschild-like power-law decay contained in $F_S \sim r_h/(2r^2)$. Using units where $r_h = 1$, the coefficient of the oscillatory terms is $O(1)$ [because $\tilde{\pi}_0 = O(1)$]. The crossing then happens when $F_S \sim 1/r_\times^2 \sim \eta/r_\times^{3/2}$, which gives $r_\times \sim \eta^{-2}$, i.e., coming back to general units

$$r_\times \sim \eta^{-2} r_h. \quad (3.28)$$

Remembering the phenomenological constraint Eq. (3.21) from Solar-System tests, we see that the crossing scale r_\times must be at least 10^{10} larger than the BH-horizon size. As, at such large distances, an astrophysical BH cannot be treated as being isolated but rather embedded within a matter distribution created by many other astrophysical objects, this suggests that the oscillatory contributions will not, in most cases, lead to identifiable observable signals. This is phenomenologically fortunate for the compatibility of the torsion-bigravity BH structure with observational data on astrophysical BHs (such as the existence and structure of accretion disks), because the dominance of the $\propto \eta r^{-3/2} \cos(\frac{\sqrt{7}}{2} \ln r + \hat{\Phi}^{F2})$ in Eq. (3.27) when $r \gtrsim r_\times$ actually means that the gravitational force $F(r) = \Phi'(r)$ generated by the BH is no longer of the standard, attractive $F \simeq r_h/(2r^2)$ type but starts oscillating around zero as $F \simeq r_h r_\times^{-1/2} r^{-3/2} \cos(\frac{\sqrt{7}}{2} \ln r + \hat{\Phi}^{F2})$. If r_\times was a distance scale where an accretion disk would be known to exist around the BH, this would phenomenologically rule out torsion-hairy BHs, because the $\ln r$ -periodic changes of sign of $F(r)$ when $r \gtrsim r_\times$ means that the gravitational force created by the BH periodically becomes repulsive, before becoming again attractive, etc.

Let us complete our discussion of the asymptotic gravitational field of torsion-hairy BHs by commenting on the presence of the logarithmic term $F_{\ln}(r) = \frac{1}{r^2} A_{(F,\ln)} \ln r$ in F . If we use again units where $r_h = 1$, we will have $A_{(F,\ln)} = O(1)$. Therefore, the ratio between $F_{\ln}(r)$ and the Schwarzschild term in (3.27) is of the order of

$$\frac{F_{\text{In}}(r)}{F_{\text{S}}(r)} \sim \eta \ln \frac{r}{r_h}. \quad (3.29)$$

In view of the phenomenological limit (3.21), this ratio is very small, even if one considers distances comparable to the crossing scale $r_{\times} \sim \eta^{-2} r_h$.

At face value, this preliminary discussion of the physical effects of the asymptotic behavior of $F(r)$ [Eq. (3.27)] seems to suggest that the Solar-System upper limit (3.21) constrains so much the magnitude of the unusual torsion-hairy gravitational field $F(r)$ that it will not lead to any observable effect. However, the more detailed discussion of the next section will show that such a conclusion would be premature.

IV. PHENOMENOLOGICAL CONSEQUENCES OF TORSION BIGRAVITY FOR SUPERMASSIVE BHS

We recalled in the introduction some of the current observational data [1–4] that probe (in a quantitative way) the structure of the gravitational field of BHs. As our current investigation of torsion bigravity is limited to the static sector, we cannot meaningfully discuss the predictions of torsion bigravity for coalescing BHs. (Such an investigation would anyway require 3D numerical simulations to be conclusive.) Here, we focus on the phenomenological consequences of the hypothetical existence³ in our Universe of torsion-hairy asymptotically flat black holes. We successively consider the observable consequences of torsion-hairy BHs for (i) the size of the shadow of BHs; (ii) the redshift of the S2 star around supermassive black hole candidate SgrA*; and (iii) the periastron precession of S2.

A. BH shadows

The 2017 Event Horizon Telescope image of Messier 87 [2] has inferred a size for the shadow of the supermassive BH at the center of Messier 87 that agrees with GR predictions within $\sim 17\%$ at the 68-percentile level. It has been emphasized in recent work [24] that this measurement offers a new test of GR that goes beyond Solar-System weak-field tests in probing the strong-field structure of gravity. As discussed in Ref. [24], the size of the BH shadow can be discussed with sufficient accuracy within the context of nonrotating, spherically symmetric BHs. It then depends only on the time-time metric component $-g_{00}(r) = e^{2\Phi(r)}$, considered as a function of the areal radius r . The shadow radius r_{sh} is given by

$$r_{\text{sh}} = r_{\text{lr}} e^{-\Phi(r_{\text{lr}})}, \quad (4.1)$$

where r_{lr} denotes the *light ring* radius (or photon-sphere radius), which is the solution of the equation

$$r_{\text{lr}} F(r_{\text{lr}}) = 1. \quad (4.2)$$

Here, as above, $F(r) = \Phi'(r)$ is the (relativistic) “gravitational force” derived from the potential $\Phi(r)$.

In view of our general result Eq. (3.26) above, we can *a priori* see that the light ring radius of torsion-hairy BHs will admit an expansion of the form

$$r_{\text{lr}}^{\text{TBG}} = r_{\text{lr}}^{\text{GR}}(r_h)(1 + a_1 \eta + O(\eta^2)), \quad (4.3)$$

where $r_{\text{lr}}^{\text{GR}}(r_h) = \frac{3}{2} r_h$ and where the coefficient a_1 is some $O(1)$ dimensionless function of the $O(1)$ shooting parameter $\tilde{\pi}_0$ describing the one-parameter family of torsion-bigravity BHs having some given horizon radius r_h . By the same reasoning, one also concludes [from Eq. (4.1)] that

$$r_{\text{sh}}^{\text{TBG}} = r_{\text{sh}}^{\text{GR}}(r_h)(1 + b_1 \eta + O(\eta^2)), \quad (4.4)$$

with another coefficient $b_1 = O(1)$.

Remembering now the strong Solar-System limit [Eq. (3.21)] on the magnitude of η and comparing it to the $\sim 17\%$ precision on the Event Horizon Telescope estimate of r_{sh} , we conclude that current (and foreseeable) shadow measurements will not bring new constraints on the torsion-bigravity theory parameter η .

As we are going to see next, the GRAVITY Collaboration *weak-field* probing of the gravitational field of the Galactic central BH candidate do provide (somewhat surprisingly) much stronger tests of torsion bigravity than the *strong-field* test provides by the Event Horizon Telescope Messier 87 observations.

B. Redshift of S2

An important observable object related to the supermassive black hole candidate SgrA* is the star S2. Its highly elliptical (eccentricity $e = 0.885$) orbit is characterized by a pericenter distance of about 1420 Schwarzschild radii and an orbital speed at the pericenter point about 2.55% of c . This makes the star S2 a sensitive probe of gravity near a black hole. Two important quantitative results based on observations of S2 were recently obtained. The first one is a measurement of the gravitational redshift of S2 along its orbit [3]. The second one is a measurement of the periastron precession of the orbit of S2 [4]. In the present subsection, we shall study how the measurements of the gravitational redshift of S2 probe the gravitational-field structure around torsion-hairy BHs.

In the following, we identify r_h (in our torsion-hairy solutions) with the measured Schwarzschild radius $r_h^{\text{obs}} = 2m_{\text{BH}} \equiv 2GM_{\text{BH}}$ of the Galactic (candidate) BH. Here M_{BH}

³We will, however, recall in the conclusions that it is not clear at this stage whether gravitational collapse in torsion bigravity will generate the type of torsion-hairy BHs studied here or, rather, ordinary GR BHs, which are also exact solutions of the torsion-bigravity field equations.

denotes the mass of the black hole expressed in kilograms or M_\odot .

The reference paper we use is Ref. [3]. In that paper, at any moment of time t , the redshift z is decomposed in the following components:

$$z(t) \equiv \frac{\Delta\lambda}{\lambda} = B_0 - \frac{v_{\text{rad}}(t)}{c} + f \left[\frac{1}{2} \frac{v_{\text{orbit}}^2(t)}{c^2} + \frac{m_{\text{BH}}}{c^2 r(t)} \right] - \Phi_{\text{TBG}}(t) + O(c^{-3}). \quad (4.5)$$

Here the radial velocity v_{rad} is the projection of the orbital velocity along the line of sight. The constant B_0 defines a constant offset. The second term (within square brackets) represents the classical GR redshift effect. It comprises two contributions: the second-order Doppler effect $\frac{1}{2} \frac{v_{\text{orbit}}^2(t)}{c^2}$ and the Einstein gravitational redshift $+\frac{m_{\text{BH}}}{c^2 r(t)}$. The parameter f was introduced in Ref. [3] as a phenomenological way to characterize the deviations between Newtonian and relativistic physics: The value $f = 0$ would correspond to purely Newtonian physics, while the value $f = 1$ corresponds to GR. By generalizing the standard derivation of the GR redshift [25], we have completed the GR result by adding, to lowest order, the additional redshift $-\Phi_{\text{TBG}}$ coming from torsion bigravity. It is defined, with our notation, as

$$\Phi_{\text{TBG}}(r) \equiv \Phi(r) - \Phi_S(r). \quad (4.6)$$

The observational results presented in Ref. [3] are summarized in the following experimental constraint on the phenomenological parameter f :

$$f = 0.90 \pm 0.09|_{\text{stat}} \pm 0.15|_{\text{sys}}. \quad (4.7)$$

As the second-order Doppler effect and the Einstein redshift are fully degenerate and have the same amplitude of variation [because of energy conservation, $\frac{1}{2} v_{\text{orbit}}^2(t) - \frac{m_{\text{BH}}}{r(t)} = \text{const}$], the constraint (4.7) means any additional redshift correction from torsion bigravity would have been visible only if it were larger than $2 \times \sqrt{0.09^2 + 0.15^2} = 0.34$ times the variation, along the orbit, of the Einstein-Schwarzschild redshift $\Phi_S \approx -\frac{m_{\text{BH}}}{r(t)} = -\frac{r_h}{2r(t)}$, namely,

TABLE I. Sample of redshift ratios and periastron ratios. The periastron ratios are computed for two different values of η , namely, $\eta = 10^{-5}$ and $\eta = 10^{-8}$.

$\bar{\pi}_0$	-250	-220	-180	-160	-100	-20	1	5.5
$\Delta\Phi_{\text{TBG}}^{\text{max}}/\Delta\Phi_S _{\eta=10^{-5}}$	0.047	0.045	0.039	0.034	0.024	0.008	0.004	0.035
$\delta\omega_{\text{TBG}}/\delta\omega_{\text{GR}} _{\eta=10^{-5}}$	154.9	85.5	19.8	1.5	-21.2	-15.0	-6.5	1.8
$\delta\omega_{\text{TBG}}/\delta\omega_{\text{GR}} _{\eta=10^{-8}}$	0.168	0.106	0.025	0.004	-0.021	-0.015	-0.006	0.003

$$\begin{aligned} \Delta\Phi_S &\equiv |\Phi_S(r_{\text{ap}}) - \Phi_S(r_{\text{per}})| = \frac{1}{2840} - \frac{1}{46550} \\ &= 3.306 \times 10^{-4}, \end{aligned} \quad (4.8)$$

where $r_{\text{ap}} = a(1+e) = r_{\text{per}} \frac{1+e}{1-e} \approx 23275r_h$ denotes the apocenter distance and $r_{\text{per}} = a(1-e) \approx 1420r_h$ the pericenter distance.

As we have shown above that the deviations from Schwarzschild's metric in torsion-hairy BHs are proportional to η (when η is small), we can consider, for concreteness, the case where $\eta = 10^{-5}$. Choosing such a specific value compatible with Solar-System tests [see Eq. (3.21)], we numerically computed the ratio

$$\frac{\Delta\Phi_{\text{TBG}}^{\text{max}}}{\Delta\Phi_S} \equiv \frac{|\Phi_{\text{TBG}}(r) - \Phi_{\text{TBG}}(r_{\text{ap}})|^{\text{max}}}{|\Phi_S(r_{\text{ap}}) - \Phi_S(r_{\text{per}})|}, \quad (4.9)$$

where the indicated maximization is done over r , as it ranges over the full orbit of S2.

After having fixed η to the value $\eta = 10^{-5}$, we still have a one-parameter family of asymptotically flat torsion-hairy BHs, described by the horizon shooting parameter $\bar{\pi}_0$. Not all values of $\bar{\pi}_0$ lead to an asymptotically flat BH. But, there is a rather large range of $\bar{\pi}_0$, namely, the interval $-289 < \bar{\pi}_0 < +5.5$, which are in the basin of attraction of the relevant attractor Eq. (2.19). We give in Table I a sample of values of the ratio $\frac{\Delta\Phi_{\text{TBG}}^{\text{max}}}{\Delta\Phi_S}$ defined in Eq. (4.9) as $\bar{\pi}_0$ varies in this allowed interval. (When $\eta = 10^{-8}$, the lower limit of the allowed interval is about -267 .) We can summarize the results of Table I in the inequality

$$0.004 \left(\frac{\eta}{10^{-5}} \right) \leq \frac{\Delta\Phi_{\text{TBG}}^{\text{max}}}{\Delta\Phi_S} \leq 0.047 \left(\frac{\eta}{10^{-5}} \right). \quad (4.10)$$

As said above, the current fractional sensitivity of redshift observations on S2 are of the order of $0.34\Delta\Phi_S$. Thus, one can conclude that, near the supermassive black hole in SgrA*, the deviation of torsion bigravity from GR has, within the current observational precision, a negligible effect on redshift measurements.

C. Periastron precession of S2

Let us now discuss the modification of the periastron precession of S2 due to the difference between torsion bigravity and GR. To compute the precession of the orbit of

a star, we start from the geodesic equation (we recall that, in torsion bigravity, massive particles follow the geodesics of $g_{\mu\nu}$ rather than autoparallels of the torsionful connection $A^\lambda_{\mu\nu}$ [17].) The geodesic equations of motion written in terms of coordinate time $t = x^0/c$ read

$$\frac{d^2 x^i}{dt^2} = - \left(\Gamma^i_{\mu\nu} - \Gamma^0_{\mu\nu} \frac{dx^i}{cdt} \right) \frac{dx^\mu}{dt} \frac{dx^\nu}{dt}. \quad (4.11)$$

Expanding the right-hand side in the usual post-Newtonian way for the GR contributions and working linearly in the additional contributions due to torsion bigravity, we can rewrite the above equations of motion as

$$\frac{d^2 x^i}{dt^2} = - \frac{m_{\text{BH}} x^i}{r^3} + a^i_{\text{GR}} + a^i_{\text{TBG}} + O(c^{-4}). \quad (4.12)$$

Here the first term is the Newtonian gravitational force and would define (if it were alone) an elliptical Keplerian trajectory without any precession. The second term represents the first post-Newtonian correction (of the order of c^{-2}) to the Newtonian force coming from the GR piece in the metric. (Here, we decompose the full metric as $g_{\mu\nu} = g^S_{\mu\nu} + h^{\text{TBG}}_{\mu\nu}$ and work linearly in the torsion-bigravity metric correction $h^{\text{TBG}}_{\mu\nu}$.) The last term represents the corrections coming from the torsion bigravity. As usual in the post-Newtonian approach, the leading-order additional contribution to the equations of motion comes only from the time-time component $c^2 h^{\text{TBG}}_{00} \approx -2c^2 \Phi_{\text{TBG}}$, where Φ_{TBG} was defined in Eq. (4.6). This leads (at leading post-Newtonian order) to

$$a^i_{\text{TBG}} = -c^2 \partial_i \Phi_{\text{TBG}}. \quad (4.13)$$

To calculate the periastron precession in the problem of motion defined by Eq. (4.12), it is convenient to use the standard Gauss form for the perturbation of Keplerian elements (see, e.g., Ref. [26]). We are interested only in the secular advance of the argument ω of the periastron. The Gauss form [see, e.g., Eq. (33), page 301 of Ref. [26]] yields $d\omega/dt$ as a linear expression in the components of the perturbing accelerating force $a^i_{\text{GR}} + a^i_{\text{TBG}}$. To leading order, we have therefore

$$\frac{d\omega}{dt} = \left(\frac{d\omega}{dt} \right)^{\text{GR}} + \left(\frac{d\omega}{dt} \right)^{\text{TBG}}, \quad (4.14)$$

where $\left(\frac{d\omega}{dt} \right)^{\text{GR}}$ is the usual GR periastron precession, whose integral over one orbit is the well-known value

$$\frac{\delta\omega^{\text{GR}}}{2\pi} = \frac{3m_{\text{BH}}}{c^2 a (1 - e^2)}. \quad (4.15)$$

The expression of the additional contribution coming from torsion bigravity simplifies in the present case where the

perturbing force a^i_{TBG} is purely radial, i.e., directed along the radial direction $n^i = \partial_i r$. It reads [26]

$$\left(\frac{d\omega}{dt} \right)^{\text{TBG}} = - \frac{(1 - e^2)^{1/2}}{nae} \cos \phi \partial_i r a^i_{\text{TBG}}. \quad (4.16)$$

Taking into account the conservation of angular momentum (per unit mass)

$$r^2 \frac{d\phi}{dt} = L = \sqrt{a(1 - e^2)m_{\text{BH}}},$$

where we used the expression for the angular momentum of the Newtonian elliptical motion and the expression of a^i_{TBG} in terms of the gradient of Φ_{TBG} [Eq. (4.13)], we get the following simple formula for the torsion-bigravity contribution to the total (reduced) periastron precession, integrated over one full period:

$$\begin{aligned} \frac{\delta\omega_{\text{TBG}}}{2\pi} &= \frac{1}{2\pi e m_{\text{BH}}} \int_0^{2\pi} \cos \phi r^2 \frac{\partial \Phi_{\text{TBG}}}{\partial r} d\phi \\ &= \frac{1}{2\pi e m_{\text{BH}}} \int_0^{2\pi} \cos \phi r^2 F_{\text{TBG}}(r) d\phi, \end{aligned} \quad (4.17)$$

where we replaced (as is allowed to leading order) Φ'_{TBG} by

$$F_{\text{TBG}}(r) \equiv F(r) - F_S(r). \quad (4.18)$$

We must now compare the value of $\frac{\delta\omega_{\text{TBG}}}{2\pi}$ to the usual GR periastron advance, Eq. (4.15). More precisely, we should compare the torsion-bigravity contribution $\frac{\delta\omega_{\text{TBG}}}{2\pi}$ to the observational accuracy with which the periastron advance has been measured.

The GRAVITY Collaboration has recently succeeded to measure the integrated periastron precession of the S2 orbit [4]. The result was presented in the form

$$\delta\omega_{\text{obs}} = f_{\text{SP}} \frac{6\pi m_{\text{BH}}}{c^2 a (1 - e^2)} = 12.1' f_{\text{SP}}, \quad (4.19)$$

where the coefficient f_{SP} was best fitted to the observations. The final result given in Ref. [4] for the coefficient f_{SP} reads

$$f_{\text{SP}} = 1.10 \pm 0.19. \quad (4.20)$$

In other words, the precision of the measurement is 19% of the GR value.

Now let us consider the contribution to periastron precession coming from the torsion-bigravity corrections. In the case (discussed above) of redshift observations, we found that torsion-hairy BHs induce (when $\eta \lesssim 10^{-5}$) only a negligible modification of the GR redshift. We might similarly expect, as all post-GR metric deviations around torsion-hairy BHs contain a factor η , so that

$F_{\text{TBG}}(r) \equiv F(r) - F_S(r) = O(\eta)$ [see Eq. (3.26)], that $\delta\omega_{\text{TBG}}$ will be automatically small compared to the error bar on $\delta\omega_{\text{obs}}$ [Eq. (4.19)]. Surprisingly, we found that this is not the case.

Calculating the torsion-bigravity contribution by combining the explicit formula Eq. (4.17) with numerical simulations of torsion-hairy BHs (depending on the choice of shooting parameter $\bar{\pi}_0$), we found that, when $\eta = 10^{-5}$, the ratio $\delta\omega_{\text{TBG}}/\delta\omega_{\text{GR}}$ ranged (as $\bar{\pi}_0$ varied) between -21 and $+160$, passing through 0 for a certain value of $\bar{\pi}_0$. A sample of our numerical results is listed in Table I.

Let us remark that, as one can see from the second line of this table, for $\eta = 10^{-5}$ and certain values of $\bar{\pi}_0$, the periastron precession per orbit is enormous: $160 \times \omega_{\text{GR}} \approx 32^\circ$. Such a large deviation from GR is totally incompatible with the recent result of the GRAVITY Collaboration.

As already said, the contribution from torsion bigravity is (approximately) proportional to the value of η . Therefore, illustrated on the last row of Table I, to pass the current tests of periastron precession one needs to take $\eta < 10^{-8}$. This shows that the periastron precession of S2 is a much more stringent test of the existence of torsion-hairy BHs than both (i) the other observations concerning supermassive BHs (redshift of S2 and shadow of Messier 87) and (ii) all Solar-System tests.

The *a priori* surprising fact that the contribution to periastron precession can exceed 100 times the GR one, while the contribution to redshift is below the experimental precision, has a simple technical explanation. Let us first recall that the gravitational redshift effect in GR is proportional to the Newtonian potential [see Eq. (4.5)], while the value of the periastron precession in GR is proportional to the first post-Newtonian, $O(\frac{1}{c^2})$, correction to the potential [see Eq. (4.15)]. By contrast, the torsion-bigravity contribution to the potential gives additional contributions *both* to the redshift [see Eq. (4.5)] and to periastron precession [see Eq. (4.17)]. [A crucial fact is that $F_{\text{TBG}}(r) \approx \Phi'_{\text{TBG}}(r)$ is *not* $\propto 1/r^2$ and, moreover, decays more slowly than $1/r^2$, so that there is a large contribution to $\delta\omega_{\text{TBG}}$ coming from the apocenter of S2.] Then, it happens that the numerical magnitude of Φ_{TBG} satisfies the following inequality:

$$\left(\frac{m_{\text{BH}}}{c^2 r}\right)^2 \ll \left(\frac{10^{-5}}{\eta}\right) \Phi_{\text{TBG}} \ll \frac{m_{\text{BH}}}{c^2 r}. \quad (4.21)$$

V. CONCLUSIONS

We continued the study, initiated in Ref. [13], of spherically symmetric black hole solutions in torsion bigravity. Reference [13] had shown that, in the infinite-range limit, these theories admit asymptotically flat black hole solutions because of the presence of attractive fixed points in the asymptotic (large- r) limit of the system of

differential equations describing the radial evolution of the metric and the torsion. We studied in detail the existence and the structure of these fixed points. By considering the Jacobian matrix of the Fuchsian-type radial evolution system near the fixed points, we discussed their attractive and repulsive character, as well as the way the metric and torsion variables approach them at large radii.

Several phenomenological aspects of asymptotically flat torsion-hairy black holes were then considered: (i) location of the light ring and of the shadow; (ii) correction to the redshift of orbiting stars; and (iii) modification of the periastron precession of orbiting stars. Previous work [22] had shown that, in the large-range limit, Solar-System tests of relativistic gravity put the severe constraint $\eta \lesssim 10^{-5}$ on the (single) theory parameter of torsion bigravity. We showed that, when $\eta = 10^{-5}$, the observable properties of asymptotically flat torsion-hairy black holes are automatically compatible with existing observational data on (a) the shadow of Messier 87 [2] and (b) the redshift of the star S2 orbiting the Galactic-center massive black hole [3]. See Eq. (4.4) and the first row of Table I.

However, we found that, when $\eta = 10^{-5}$, the one-parameter family of asymptotically flat torsion-hairy black holes (parametrized by the horizon parameter $\bar{\pi}_0$) generically induce an additional (post-GR) contribution to the periastron precession of S2 which is typically much larger than the Schwarzschild precession. See the second row of Table I. Barring a fine-tuning of the value of the horizon shooting parameter $\bar{\pi}_0$, we concluded that the current measurements of the periastron precession of S2 [4] are about 1000 times more stringent than Solar-System gravitational tests and constrain the torsion-bigravity theory parameter η to be (see the third row of Table I)

$$\eta \lesssim 10^{-8}. \quad (5.1)$$

The physical reasons behind this surprisingly stringent probing power of periastron precession are briefly discussed at the end of Sec. IV [see, notably, Eq. (4.21)]. It is generally expected (given current Solar-System tests of weak-field gravity) that non-GR black holes will differ from GR ones mostly in the near-horizon, strong-field regime [24]. We note that torsion-hairy black holes offer a counterexample to this expectation. Though their observable predictions tend to the GR ones as $\eta \rightarrow 0$, the fact that the torsion-bigravity gravitational field $F_{\text{TBG}}(r) \equiv F(r) - F_{\text{GR}}(r)$ decays, at large radii, in a slower than $1/r^2$ manner [namely, $\propto \eta r^{-3/2} \cos(\frac{\sqrt{7}}{2} \ln r + \hat{\Phi}^{F^2})$; see Eq. (3.27)] makes the periastron precession of S2 (whose orbit ranges between 1420 Schwarzschild radii and 23275 Schwarzschild radii) a very sensitive probe of torsion-hairy black holes.

Let us also emphasize again that, contrary to what has been assumed in previous phenomenological discussions of possible observable effects of spacetime torsion [27,28], the post-GR observable effects of torsion-hairy black holes

are not directly related to the torsion field around these black holes. Our results in Sec. II allow one to derive the large- r behavior of the two independent components of the contorsion tensor, K_{100} and K_{122} . For instance, we have [using Eqs. (5.9) in Ref. [13]]

$$K_{122}(r) = \left(\tilde{w}(r) - \frac{1}{l(r)} \right) W_S(r), \quad (5.2)$$

so that Eqs. (3.18) and (3.25) above yield an asymptotic radial decay of $K_{122}(r)$ of the form

$$K_{122}(r) = +\frac{2}{r} + O\left(\frac{\cos\left(\frac{\sqrt{7}}{2}\ln r + \Phi^K\right)}{r^{3/2}}\right). \quad (5.3)$$

However, this contorsion field, as well as the companion

$$K_{100}(r) = O\left(r^{-3/2} \cos\left(\frac{\sqrt{7}}{2}\ln r + \Phi^K\right)\right), \quad (5.4)$$

does not play a direct role in modifying the motion of orbiting stars. Indeed, test bodies in torsion bigravity follow geodesics of the spacetime metric $g_{\mu\nu}$ and not autoparallels of the torsionful connection $A^{\lambda}_{\mu\nu}$ [17]. (One would need to have spin-polarized elementary fermions to directly probe the torsion hair.) However, the presence of a propagating torsion field modifies the field equations and, thereby, indirectly modifies the structure of the metric $g_{\mu\nu}$. It is then the latter torsion-induced metric modifications that have induced the slowly decaying (and oscillating) contributions to the gravitational force $F(r) = F_S(r) + F_{\text{TBG}}(r)$ responsible for the unexpectedly large contributions to the periastron precession of S2.

As a final comment, let us emphasize that the very strong experimental constraint Eq. (5.1) on the torsion-bigravity theory parameter η has been derived in the present work under the following two basic assumptions: (i) a vanishingly small inverse range κ and (ii) real astrophysical black holes are described by the asymptotically flat torsion-hairy black hole solutions of torsion bigravity. The second assumption would be justified only if one proves that the collapse of a torsion-hairy star [22] in torsion bigravity does dynamically generate a torsion-hairy black hole rather than an ordinary GR black hole (which is also an exact solution of torsion bigravity). It is quite possible (especially in view of the fact that Schwarzschild black holes cannot support an infinitesimal torsion hair [13]) that the torsion hair of a torsion-hairy star will be radiated away during the collapse. Another angle for clarifying this issue is to study the dynamical stability of Schwarzschild black holes within the context of torsion bigravity. If, similarly to what was found in bimetric gravity [29,30], Schwarzschild black holes turn out to be unstable for small enough values of κr_h , this will suggest that the torsion-hairy black holes considered here will be the ultimate outcome of gravitational collapse. We leave this important issue to future work.

ACKNOWLEDGMENTS

I thank Thibault Damour for informative discussions.

APPENDIX A: DEFINITIONS OF SOME BASIC QUANTITIES IN USE

The static, spherically symmetric metric (2.1) naturally defines a corresponding orthonormal polar-type coframe $\theta^{\hat{i}} = e^{\hat{i}}_{\mu} dx^{\mu}$, as well as a corresponding frame $e_{\hat{i}}^{\mu} \partial/\partial x^{\mu}$, where we use hatted Latin letters to denote the frame indices. The coframe reads as follows:

$$\theta^{\hat{0}} = e^{\Phi} dt, \quad \theta^{\hat{1}} = L dr, \quad \theta^{\hat{2}} = r d\theta, \quad \theta^{\hat{3}} = r \sin\theta d\phi. \quad (\text{A1})$$

It is technically convenient to work not with coordinate components but with components with respect to the vierbein (A1). In particular, we work with the vierbein components $A^{\hat{i}}_{\hat{j}\hat{k}} = A^{\hat{i}}_{\hat{j}\mu} e_{\hat{k}}^{\mu}$ of the torsionful affine connection one-form $\mathcal{A}^{\hat{i}}_{\hat{j}} = A^{\hat{i}}_{\hat{j}\mu} dx^{\mu}$ instead of working with its coordinate components $A^{\lambda}_{\nu\mu}$ (which are related to the vierbein components $A^{\hat{i}}_{\hat{j}\hat{k}}$ by well-known relations involving the derivative of the vierbein). The affine connection one-form $\mathcal{A}^{\hat{i}}_{\hat{j}}$ defines the curvature two-form $\mathcal{F}^{\hat{i}}_{\hat{j}} = \frac{1}{2} F^{\hat{i}}_{\hat{j}\mu\nu} dx^{\mu} \wedge dx^{\nu}$ as follows:

$$\mathcal{F}^{\hat{i}}_{\hat{j}} = dA^{\hat{i}}_{\hat{j}} + \mathcal{A}^{\hat{i}}_{\hat{s}} \wedge \mathcal{A}^{\hat{s}}_{\hat{j}}, \quad (\text{A2})$$

which reads more explicitly

$$F^{\hat{i}}_{\hat{j}\mu\nu} = \partial_{\mu} A^{\hat{i}}_{\hat{j}\nu} - \partial_{\nu} A^{\hat{i}}_{\hat{j}\mu} + A^{\hat{i}}_{\hat{m}\mu} A^{\hat{m}}_{\hat{j}\nu} - A^{\hat{i}}_{\hat{m}\nu} A^{\hat{m}}_{\hat{j}\mu}. \quad (\text{A3})$$

The (curvature) frame components $F^{\hat{i}}_{\hat{j}\hat{k}\hat{l}}$ of $\mathcal{F}^{\hat{i}}_{\hat{j}}$ are then defined as

$$F^{\hat{i}}_{\hat{j}\hat{k}\hat{l}} = e_{\hat{k}}^{\mu} e_{\hat{l}}^{\nu} F^{\hat{i}}_{\hat{j}\mu\nu}. \quad (\text{A4})$$

The frame components of the corresponding Ricci tensor, $F_{\hat{i}\hat{j}} = e_{\hat{i}}^{\mu} e_{\hat{j}}^{\nu} F_{\mu\nu}$, are then defined as usual, namely, $F_{\hat{i}\hat{j}} = F^{\hat{s}}_{\hat{i}\hat{s}\hat{j}}$.

The affine connection we work with in this model is *metric preserving* which is characterized by the condition $A_{\hat{i}\hat{j}\mu} = -A_{\hat{j}\hat{i}\mu}$, where $A_{\hat{i}\hat{j}\mu} \equiv \eta_{\hat{i}\hat{s}} A^{\hat{s}}_{\hat{j}\mu}$. In the static, spherically symmetric, and parity-preserving case which we consider, the torsionful connection can be parametrized by two radial functions, $V(r)$ and $W(r)$, which are defined, respectively, as

$$V \equiv A^{\hat{1}}_{\hat{0}\hat{0}} \quad (\text{A5})$$

and

$$W \equiv A^{\hat{1}}_{\hat{2}\hat{2}} = A^{\hat{1}}_{\hat{3}\hat{3}}. \quad (\text{A6})$$

**APPENDIX B: EXPLICIT FORM OF THE
FIELD EQUATIONS OF STATIC,
SPHERICALLY SYMMETRIC
TORSION BIGRAVITY**

$$F = \{3 - 3r + 2(r-1)\eta\tilde{l}[-6 + (1+\eta)\bar{\pi}]\tilde{w} - \tilde{l}^2[2r\eta(1+\eta)\bar{\pi} + k^2r^3\eta(1+\eta)\bar{\pi}^2 - 3(r(1+\eta) + 3(r-1)\eta\tilde{w}^2)]\} / \times \{2(r-1)r[3 + \eta\tilde{l}(3 + (1+\eta)\bar{\pi})\tilde{w}]\}, \quad (\text{B1}) \quad \text{where}$$

$$\frac{d}{dr}\bar{\pi}(\tilde{l}, \tilde{w}, \bar{\pi}) = \frac{3 - 3\tilde{l}\tilde{w} - (1+\eta)\bar{\pi}(2 + \tilde{l}\tilde{w})}{r(1+\eta)}, \quad (\text{B2})$$

$$\frac{d}{dr}\tilde{l}(\tilde{l}, \tilde{w}, \bar{\pi}) = \frac{N_{\tilde{l}}}{D_{\tilde{l}}}, \quad (\text{B3})$$

$$\frac{d}{dr}\tilde{w}(\tilde{l}, \tilde{w}, \bar{\pi}) = \frac{N_{\tilde{w}}}{D_{\tilde{w}}}, \quad (\text{B4})$$

$$\begin{aligned} N_{\tilde{l}} &= \tilde{l}\{9[9(r+4\eta-3r\eta) + 12(r-1)\eta(1+\eta)\bar{\pi} + (r-2)\eta(1+\eta)^2\bar{\pi}^2] - 3\eta\tilde{l}[27(5+6r(\eta-1)-7\eta) \\ &\quad - 9(1+\eta)(1+(-3+4r)\eta)\bar{\pi} - 3(-9+8r)\eta(1+\eta)^2\bar{\pi}^2 + (-1+2r)\eta(1+\eta)^3\bar{\pi}^3]\tilde{w} \\ &\quad + 2\eta\tilde{l}^3(3+(1+\eta)\bar{\pi})\tilde{w}[\kappa^2r^3\eta(1+\eta)^2(-1+2\eta)\bar{\pi}^3 + 3\eta(1+\eta)^2\bar{\pi}^2(\kappa^2r^3+2r\eta-2(r-1)\eta\tilde{w}^2) \\ &\quad + 27(-r(1+\eta)^2+(r-1)(\eta-1)\eta\tilde{w}^2) - 9\eta(1+\eta)\bar{\pi}(r(-1+\kappa^2r^2-\eta)+(r-1)(1+\eta)\tilde{w}^2)] \\ &\quad + 3\tilde{l}^2[2r\eta(1+\eta)^2(\eta(1+\eta)+\kappa^2r^2(-1+2\eta))\bar{\pi}^3 + \kappa^2r^3\eta^2(1+\eta)^3\bar{\pi}^4 \\ &\quad + 18\eta(1+\eta)\bar{\pi}(-\kappa^2r^3+(r-1)(\eta-1)\tilde{w}^2) - 3\eta(1+\eta)^2\bar{\pi}^2(r+\kappa^2r^3-3r\eta+11(r-1)\eta\tilde{w}^2) \\ &\quad + 27(-r(1+\eta)^2+(r-1)\eta(1+13\eta)\tilde{w}^2)]\}, \\ D_{\tilde{l}} &= 6(1-r)r(1+\eta)(-9+\eta(1+\eta)\bar{\pi}^2)[3+\eta\tilde{l}(3+(1+\eta)\bar{\pi})\tilde{w}], \\ N_{\tilde{w}} &= \kappa^2r^3\eta^2(1+\eta)^4\tilde{l}^3\bar{\pi}^5\tilde{w} - 9(1+\eta)^2\bar{\pi}^2[2-2r+(8-9r)\eta\tilde{l}\tilde{w} + \eta\tilde{l}^3\tilde{w}(r+3\kappa^2r^3-3r\eta+3(-1+r)\eta\tilde{w}^2) \\ &\quad + \tilde{l}^2(2r(1+2\kappa^2r^2-\eta)+(-9+10r)\eta\tilde{w}^2)] + 81[4-4r+(-6+5r+6\eta-7r\eta)\tilde{l}\tilde{w} - \eta(13-12r+\eta)\tilde{l}^2\tilde{w}^2 \\ &\quad + \tilde{l}^3\tilde{w}(-r(1+\eta)^2+(-1+r)(-3+\eta)\eta\tilde{w}^2)] + \eta(1+\eta)^3\tilde{l}^2\bar{\pi}^4\{6\kappa^2r^3+\eta(1+\eta)\tilde{w}^2 + \tilde{l}\tilde{w}[r(2\eta(1+\eta) \\ &\quad + \kappa^2r^2(-2+7\eta)) - 2(-1+r)\eta(1+\eta)\tilde{w}^2]\} + 3(1+\eta)^2\tilde{l}\bar{\pi}^3\{-(-2+r)\eta(1+\eta)\tilde{w} \\ &\quad + \eta\tilde{l}^2\tilde{w}(r(-1+3\kappa^2r^2(-1+\eta)+4\eta+5\eta^2) - 5(-1+r)\eta(1+\eta)\tilde{w}^2) + 2\tilde{l}[r(2\eta(1+\eta)+\kappa^2r^2(-1+2\eta)) \\ &\quad - (-1+r-\eta)\eta(1+\eta)\tilde{w}^2]\} - 27(1+\eta)\bar{\pi}[4-4r+(r+4\eta-3r\eta)\tilde{l}\tilde{w} + \tilde{l}^3\tilde{w}(r(1+2\eta+2\kappa^2r^2\eta+\eta^2) \\ &\quad - (-1+r)(-3+\eta)\eta\tilde{w}^2) + 2\tilde{l}^2(r(1+\kappa^2r^2+\eta)+\eta(3-2r+\eta)\tilde{w}^2)], \\ D_{\tilde{w}} &= 2(1-r)r(1+\eta)\tilde{l}(3+(1+\eta)\bar{\pi})(-9+\eta(1+\eta)\bar{\pi}^2)[3+\eta\tilde{l}(3+(1+\eta)\bar{\pi})\tilde{w}]. \end{aligned} \quad (\text{B5})$$

- [1] B. Abbott *et al.* (LIGO Scientific and Virgo Collaborations), Tests of general relativity with the binary black hole signals from the LIGO-Virgo catalog GWTC-1, *Phys. Rev. D* **100**, 104036 (2019).
[2] K. Akiyama *et al.* (Event Horizon Telescope Collaboration), First M87 Event Horizon Telescope results. I. The shadow of the supermassive black hole, *Astrophys. J.* **875**, L1 (2019).
[3] R. Abuter *et al.* (GRAVITY Collaboration), Detection of the gravitational redshift in the orbit of the star S2 near the

Galactic centre massive black hole, *Astron. Astrophys.* **615**, L15 (2018).

- [4] R. Abuter *et al.* (GRAVITY Collaboration), Detection of the Schwarzschild precession in the orbit of the star S2 near the Galactic centre massive black hole, *Astron. Astrophys.* **636**, L5 (2020).
[5] E. Berti *et al.*, Testing general relativity with present and future astrophysical observations, *Classical Quantum Gravity* **32**, 243001 (2015).

- [6] E. Barausse and T. P. Sotiriou, Perturbed Kerr Black Holes can Probe Deviations from General Relativity, *Phys. Rev. Lett.* **101**, 099001 (2008).
- [7] T. P. Sotiriou and S. Y. Zhou, Black Hole Hair in Generalized Scalar-Tensor Gravity, *Phys. Rev. Lett.* **112**, 251102 (2014).
- [8] D. D. Doneva and S. S. Yazadjiev, New Gauss-Bonnet Black Holes with Curvature-Induced Scalarization in Extended Scalar-Tensor Theories, *Phys. Rev. Lett.* **120**, 131103 (2018).
- [9] H. O. Silva, J. Sakstein, L. Gualtieri, T. P. Sotiriou, and E. Berti, Spontaneous Scalarization of Black Holes and Compact Stars from a Gauss-Bonnet Coupling, *Phys. Rev. Lett.* **120**, 131104 (2018).
- [10] R. Brito, V. Cardoso, and P. Pani, Black holes with massive graviton hair, *Phys. Rev. D* **88**, 064006 (2013).
- [11] E. Babichev and R. Brito, Black holes in massive gravity, *Classical Quantum Gravity* **32**, 154001 (2015).
- [12] J. Enander and E. Mortsell, On stars, galaxies and black holes in massive bigravity, *J. Cosmol. Astropart. Phys.* **11** (2015) 023.
- [13] V. Nikiforova and T. Damour, Black holes in torsion bigravity, *Phys. Rev. D* **102**, 084027 (2020).
- [14] E. Sezgin and P. van Nieuwenhuizen, New ghost free gravity Lagrangians with propagating torsion, *Phys. Rev. D* **21**, 3269 (1980).
- [15] E. Sezgin, Class of ghost free gravity Lagrangians with massive or massless propagating torsion, *Phys. Rev. D* **24**, 1677 (1981).
- [16] K. Hayashi and T. Shirafuji, Gravity from poincare gauge theory of the fundamental particles. 1. General formulation, *Prog. Theor. Phys.* **64**, 866 (1980); Erratum, *Prog. Theor. Phys.* **65**, 2079 (1981).
- [17] K. Hayashi and T. Shirafuji, Gravity from poincare gauge theory of the fundamental particles. 2. Equations of motion for test bodies and various limits, *Prog. Theor. Phys.* **64**, 883 (1980); Erratum, *Prog. Theor. Phys.* **65**, 2079 (1981).
- [18] K. Hayashi and T. Shirafuji, Gravity from poincare gauge theory of the fundamental particles. 3. Weak field approximation, *Prog. Theor. Phys.* **64**, 1435 (1980); Erratum, *Prog. Theor. Phys.* **66**, 741 (1981).
- [19] K. Hayashi and T. Shirafuji, Gravity from poincare gauge theory of the fundamental particles. 4. Mass and energy of particle spectrum, *Prog. Theor. Phys.* **64**, 2222 (1980).
- [20] S. F. Hassan and R. A. Rosen, Bimetric gravity from ghost-free massive gravity, *J. High Energy Phys.* **02** (2012) 126.
- [21] V. Nikiforova, S. Randjbar-Daemi, and V. Rubakov, Infrared modified gravity with dynamical torsion, *Phys. Rev. D* **80**, 124050 (2009).
- [22] T. Damour and V. Nikiforova, Spherically symmetric solutions in torsion bigravity, *Phys. Rev. D* **100**, 024065 (2019).
- [23] V. Nikiforova, Absence of a Vainshtein radius in torsion bigravity, *Phys. Rev. D* **101**, 064017 (2020).
- [24] D. Psaltis *et al.* (EHT Collaboration), Gravitational Test Beyond the First Post-Newtonian Order with the Shadow of the M87 Black Hole, *Phys. Rev. Lett.* **125**, 141104 (2020).
- [25] E. Schrödinger, *Expanding Universes*, 1st paperback ed. (Cambridge University Press, Cambridge, England, 2010), p. 93.
- [26] D. Brouwer and G. M. Clemence, *Methods of Celestial Mechanics* (Academic, New York, 1961).
- [27] Y. Mao, M. Tegmark, A. H. Guth, and S. Cabi, Constraining torsion with gravity probe B, *Phys. Rev. D* **76**, 104029 (2007).
- [28] R. March, G. Bellettini, R. Tauraso, and S. Dell’Agnello, Constraining spacetime torsion with the Moon and Mercury, *Phys. Rev. D* **83**, 104008 (2011).
- [29] E. Babichev and A. Fabbri, Instability of black holes in massive gravity, *Classical Quantum Gravity* **30**, 152001 (2013).
- [30] R. Brito, V. Cardoso, and P. Pani, Massive spin-2 fields on black hole spacetimes: Instability of the Schwarzschild and Kerr solutions and bounds on the graviton mass, *Phys. Rev. D* **88**, 023514 (2013).